Journal of Alloys and Compounds 509 (2011) 5300–5304

Contents lists available at ScienceDirect

Journal of Alloys and Compounds

journal homepage: www.elsevier.com/locate/jallcom

Effect of Ca-doping on the structural and electrical properties of $CuY_{1-x}Ca_xO_2$ ($0 \le x \le 0.10$) ceramics

Zanhong Deng[a,b,*], Xiaodong Fang[a,b], Ruhua Tao[a,b], Weiwei Dong[a,b], Shu Zhou[a,b], Gang Meng[a,b], Jingzhen Shao[a,b]

[a] Anhui Provincial Key Lab of Photonics Devices and Materials, Anhui Institute of Optics and Fine Mechanics, Chinese Academy of Sciences, Hefei 230031, PR China
[b] Key Lab of New Thin Film Solar Cells, Chinese Academy of Sciences, Hefei 230031, PR China

ARTICLE INFO

Article history:
Received 6 July 2010
Received in revised form 21 January 2011
Accepted 27 January 2011
Available online 12 February 2011

Keywords:
Semiconductors
Oxide materials
Solid state reaction
Electronic properties

ABSTRACT

Delafossites $CuY_{1-x}Ca_xO_2$ ($0 \le x \le 0.10$) ceramics have been prepared by solid state reaction using Cu_2O, Y_2O_3 and $CaCO_3$. Liquid phase sintering, which obviously accelerates the reaction speed of Cu_2O–Y_2O_3–$CaCO_3$ system and promotes the formation of $CuYO_2$ phase is evidenced for the Ca-doped samples. During the sintering process, CuO can react with CaO to form two intermediate compounds, $CaCu_2O_3$ and Ca_2CuO_3, which decompose into CaO and liquid phase during 1273–1323 K. In the dopant range of $0 \le x \le 0.10$, both electrical conductivity and density of the samples are increased by Ca-doping. The room temperature conductivity of $CuY_{0.94}Ca_{0.06}O_2$ is more than four orders of magnitude higher than that of $CuYO_2$.

1. Introduction

Delafossite oxides ABO_2 (A is Cu and Ag, B is trivalent cation, such as Al, Cr, Y, La, Sc) have been studied intensively due to their applications as catalysts [1–3], sensors [4,5], diluted magnetic semiconductors [6] and transparent p-type conducting oxides (p-TCOs) [7–10]. As the key components of all-oxide transparent devices, the p-TCOs have potential applications in the so called "invisible circuits" [11]. However, the conductivities of these p-TCOs are much lower than those of n-TCOs, such as tin-doped indium oxide (ITO), ZnO [12]. With the aim to enhance p-type conductivities, acceptor-doping on B-site as well as nonstoichiometric (excess oxygen and/or excess metal cations) in these delafossite oxides are interesting to be studied [13–17].

The delafossite structure can be described as sheets of edge-shared BO_6 octahedra alternating stacked with close-packed A-ions layers. Delafossites ABO_2 can form either rhombohedral 3R ($R\bar{3}m$) or hexagonal 2H ($P6_3/mmc$) structures, depending on the stacking of the layers [18]. In the previous studies, the crystal structure, luminescence property and thermoelectric power of $CuYO_2$ were studied; its application to p-TCOs and hydrogen photocathode was explored [19–22]. Ca^{2+} doped $CuYO_2$ has also been reported in the previous studies [23–25]. Singh et al. have analyzed the thermopower and related properties of doped $CuYO_2$ and suggested that Ca^{2+} doping in the Y site was less likely to produce strong scattering. Study on luminescence properties by Tsuboi et al. showed that for $CuY_{1-x}Ca_xO_2$ ($0 \le x \le 0.05$), with the increase in Ca concentration, the Cu^+ emission shifted slightly to the shorter-wavelength side which was considered to be caused by the increase in hole concentration. They have also found that the p-type conductivity of $CuR_xCa_yY_{1-x-y}O_2$ ($x = 0.005$ and $y \le 0.02$) increased with increasing Ca concentration, indicating the increase of hole concentration caused by doping with Ca^{2+} acceptor cation on the Y^{3+} site. Ingram has reported significant increase in the hole concentration of $CuY_{0.95}Ca_{0.05}O_2$ relative to the undoped compound, however the hole contents were less than expected based upon the doping level, second phases (e.g., CaO) were assumed to exist in small proportions though they were undetectable in XRD analysis.

It is reported that the Ca^{2+} doped $CuYO_2$ thin film prepared by thermal co-evaporation showed a bandgap of 3.5 eV, average transparency of 50% in the visible region and enhanced p-type conductivity of 1.0 S cm^{-1}.

In this article, a series of $CuY_{1-x}Ca_xO_2$ ($0 \le x \le 0.10$) ceramics were prepared by solid-state reaction technique using Cu_2O, Y_2O_3 and $CaCO_3$. The role of $CaCO_3$ in the reaction system of Cu_2O–Y_2O_3–$CaCO_3$ was studied. The effect of Ca-doping on the structural and electrical properties of $CuYO_2$ was investigated.

* Corresponding author. Tel.: +86 551 5593508; fax: +86 551 5593527.
E-mail address: zhdeng@aiofm.ac.cn (Z. Deng).

0925-8388/$ – see front matter © 2011 Elsevier B.V. All rights reserved.
doi:10.1016/j.jallcom.2011.01.184

2. Experimental

Polycrystalline samples of delafossites $CuY_{1-x}Ca_xO_2$ ($0 \le x \le 0.10$) were prepared by solid-state reaction technique. The starting materials were Cu_2O (Alfa Aesar, 99.0%), Y_2O_3 (Alfa Aesar, 99.9%) and $CaCO_3$ (Alfa Aesar, 99.0%). Y_2O_3 was dried at 1073 K under air atmosphere for 8 h before use. The stoichiometric mixtures of Cu_2O, Y_2O_3 and $CaCO_3$ were grinded and sintered at 1373 K for 10 h under N_2 atmosphere, respectively. The grinding and sintering procedures were repeated twice. Then the powders were grinded, pelleted and annealed at 1373 K for 10 h under N_2 atmosphere, respectively, to obtain pure delafossite phase. Note that the N_2 gas stream was cut off when all the samples were cooled to 473 K. All the pellets were pressed under the same pressure of about 35 MPa and annealed in a batch in order to exclude the influence of experimental factors on the electrical properties.

A Philips X'pert PRO X-ray diffractometer (XRD) with Cu-Kα source was used to identify the crystalline phases. Diffraction patterns were taken from 10 to 80° at a scanning speed of 4°/min. The lattice parameters were calculated by the least square method from the diffraction peaks (0 0 2), (1 0 0), (1 0 1), (0 0 4), (1 0 2), (1 0 4), (1 1 0), (1 0 6) and (1 1 4) of the 2H–$CuYO_2$ phase. The theoretical densities were calculated from the lattice parameters. Though the absolute value of the lattice parameters and theoretical densities may not be accurate, the relative variations of the parameters could provide valuable information.

A FEI designed Sirion 200 field-emission scanning electron microscope (FE-SEM) was used to check the crystallization and microstructures. The temperature dependence of the conductivity was measured by the standard four-probe method by means of the cryogenic refrigeration equipment.

3. Results and discussion

XRD analysis was performed on the $CuY_{1-x}Ca_xO_2$ ($0 \le x \le 0.10$) samples which were prepared under the same sintering temperature of 1373 K for 20 h. For the samples of $0.02 \le x \le 0.10$, all diffraction peaks are indexed as the 2H–$CuYO_2$ phase (JCPDF No. 76-1422) and no secondary phase can be detected, as shown in Fig. 1. For the sample of $x = 0$, the diffraction peaks of original material Y_2O_3 can be found. Further sintering the sample at 1453 K for 10 h still can detect some Y_2O_3 phase. This means that $CaCO_3$ can obviously accelerate the reaction speed of the Cu_2O and Y_2O_3, and then decrease the sintering temperature of $CuYO_2$. In addition, the gradual shifting to lower angle was observed on the XRD pattern peaks for the calcium doped samples. That may be associated with the solid solution of Ca^{2+} into the $CuYO_2$ lattice, due to the substitution of Ca^{2+} ions with a large ionic radius (0.99 Å) for Y^{3+} (0.89 Å). Indeed, the lattice parameters (Fig. 2) obtained from XRD patterns increase with the Ca-doping amounts x for $0 \le x \le 0.06$, but further increase of the x makes negligible elongation of the lattice parameters suggesting a solubility limit of 0.06, which agrees with the inference proposed above. Secondary phases (e.g., CaO) may be undetectable by XRD analysis, but are assumed to exist in small proportions in the sample of $x = 0.10$. For sample $x = 0$, some diffraction peaks of original material Y_2O_3 may overlap with that of 2H–$CuYO_2$ and result in larger error than those of other samples in lattice parameters calculation. That may be the reason for the lattice parameters decrease from $x = 0$ to 0.02.

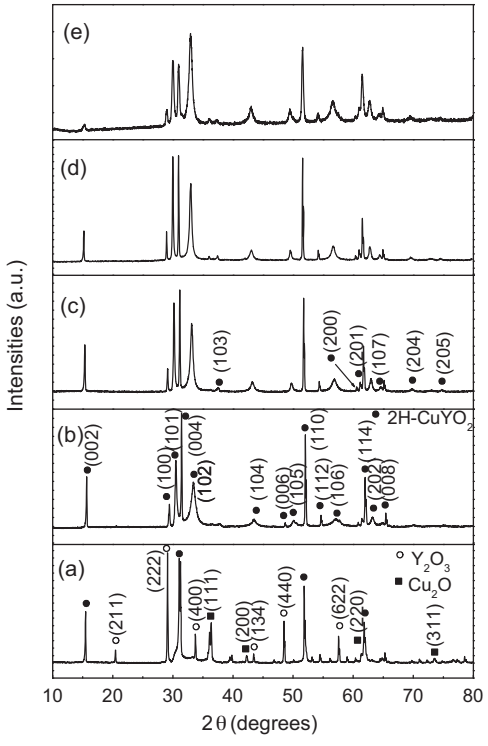

Fig. 1. XRD patterns of the $CuY_{1-x}Ca_xO_2$ ($0 \le x \le 0.10$) samples: (a) $x = 0$; (b) $x = 0.02$; (c) $x = 0.04$; (d) $x = 0.06$; (e) $x = 0.10$.

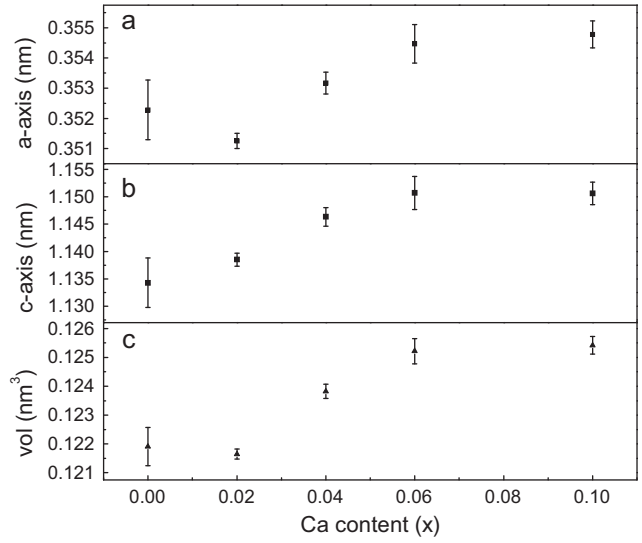

Fig. 2. Lattice parameters of the $CuY_{1-x}Ca_xO_2$ ($0 \le x \le 0.10$) samples.

SEM analysis was performed to check the microstructures, as shown in Fig. 3. The particles of the undoped sample exhibit an irregular morphology consisting of particles around 1 μm with some agglomeration, as shown in the Fig. 3(a). The morphologies of the Ca-doped samples, which are absolutely different from the undoped sample with much larger particles compactly connected to each other, suggest liquid phase sintering taking place. The liquid phase sintering obviously accelerates the reaction speed of Cu_2O–Y_2O_3–$CaCO_3$ system and promotes the formation of $CuYO_2$ phase. It also contributes to the increase of relative density from about 67% for the undoped sample to around 80% for the Ca-doped samples.

Since the liquid phase may be obtained by the reaction of system $CaCO_3$–Cu_2O or Y_2O_3–$CaCO_3$ at 1373 K, a series of experiments were designed to figure out the origin of liquid phase, as shown in Table 1. Cu_2O–Y_2O_3 (labeled as S2), $CaCO_3$–Y_2O_3 (labeled as S3) and $CaCO_3$–Cu_2O (labeled as S4) were sintered at 1323 K under N_2 atmosphere, respectively. Only sample S4, which is mainly composed of CaO and Cu_2O phases, shows the sign of liquid phase sintering as shown in Figs. 4 and 5. Gadalla [26] and Hou [27] reported that in the system CuO–Cu_2O–CaO ($CaCO_3$), $CaCO_3$ decomposed completely into CaO and CO_2 below 1073 K, then CuO and CaO could react to form two intermediate compounds, $CaCu_2O_3$ and Ca_2CuO_3, which decomposed into CaO and liquid phase during 1273–1323 K. Under the reduced oxygen condition of our experiments, the formation of $CaCu_2O_3$ and Ca_2CuO_3 is also evidenced in the system $CaCO_3$–Cu_2O at 1123 K (labeled as S5) as shown in Fig. 6. The formation of liquid phase during the sintering process obviously accelerates the formation of $CuYO_2$ phase and decreases the porosity.

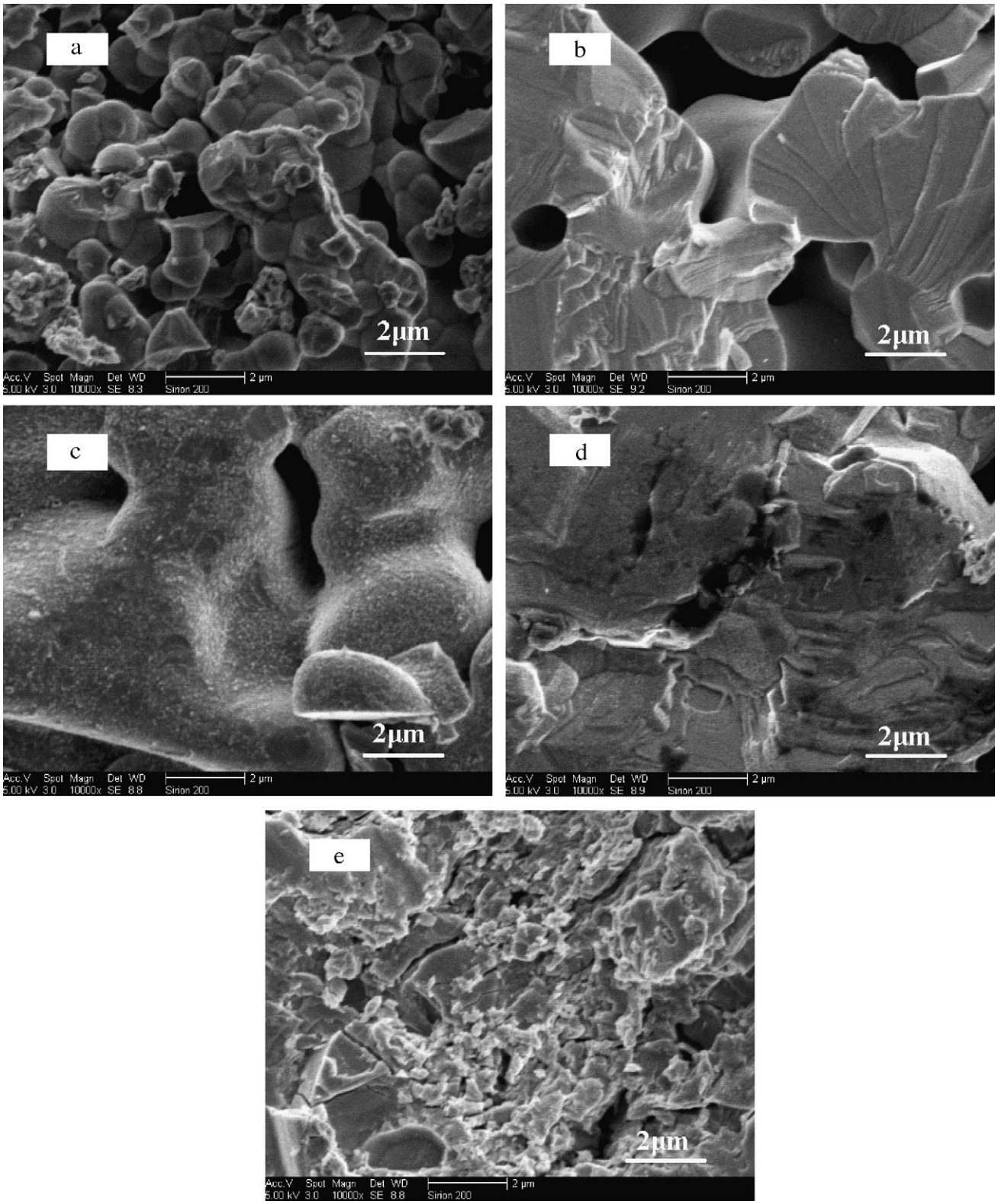

Fig. 3. SEM images of the $CuY_{1-x}Ca_xO_2$ ($0 \le x \le 0.10$) samples: (a) $x = 0$; (b) $x = 0.02$; (c) $x = 0.04$; (d) $x = 0.06$; (e) $x = 0.10$.

The temperature dependences of electrical conductivities are shown in Fig. 7. Electrical conductivities increase with the increase of temperature over the measured temperature range, indicating semiconducting behavior. It is reported that Ca-doping could enhance the electrical conductivity of $CuYO_2$ by introducing positive holes [19,21,23–25,28]. In our experiment, the conductivities increase with the dopant concentration x when $0 \le x \le 0.06$ and then decrease with x when $0.06 \le x \le 0.10$, which may be ascribed to second phase formation. Moreover, it is observed that the room temperature conductivity of the sample with $x = 0.06$ (5.11×10^{-3} S cm^{-1}) is more than four orders of magnitude higher than that of the sample with $x = 0$ (1.18×10^{-7} S cm^{-1}).

Table 1
Sintering conditions of samples S1–S5.

No.	Starting materials	Molar ratio	Reaction conditions	Liquid phase sintering?
S1	Cu_2O–Y_2O_3–$CaCO_3$	Cu:Y:Ca = 1:0.9:0.1	1323 K, N_2, 12 h	Yes
S2	Cu_2O–Y_2O_3	Cu:Y = 1:1	1323 K, N_2, 12 h	No
S3	$CaCO_3$–Y_2O_3	Ca:Y = 1:1	1323 K, N_2, 12 h	No
S4	$CaCO_3$–Cu_2O	Ca:Cu = 1:1	1323 K, N_2, 12 h	Yes
S5	$CaCO_3$–Cu_2O	Ca:Cu = 1:1	1123 K, N_2, 12 h	No

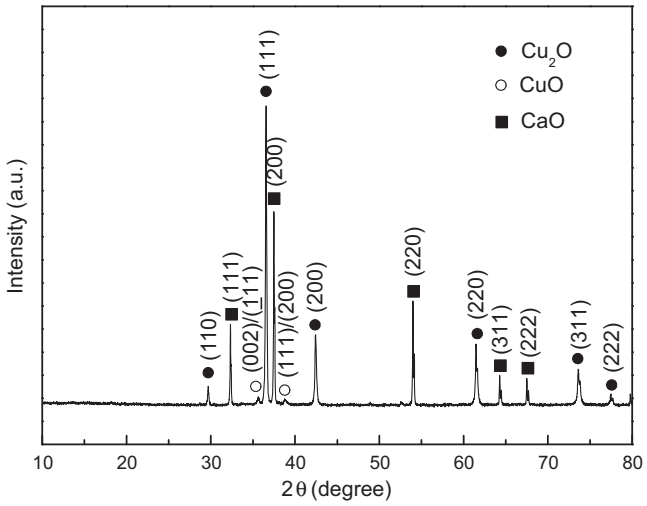

Fig. 4. XRD pattern of sample S4.

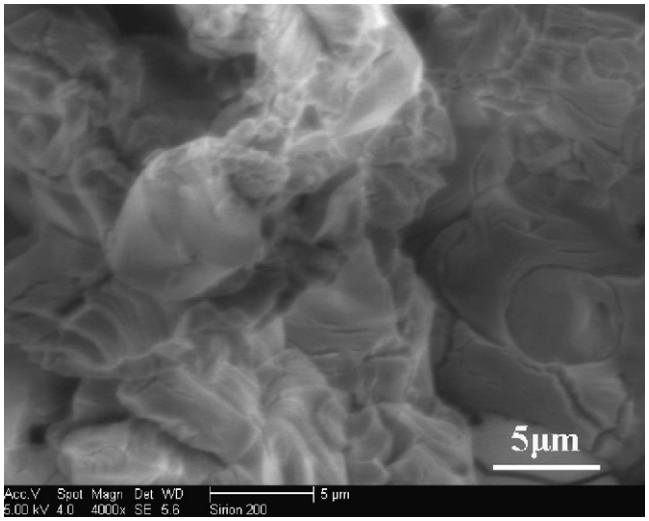

Fig. 5. SEM image of sample S4.

4. Conclusions

The effect of Ca-doping on the structural and electrical properties of $CuYO_2$ ceramics is studied. By introducing $CaCO_3$ into the system Cu_2O–Y_2O_3, intermediate liquid phase is formed by the reaction of Cu_2O and CaO during the sintering process, which obviously accelerates the reaction speed of Cu_2O–Y_2O_3–$CaCO_3$ system and promotes the formation of $CuYO_2$ phase, the porosity is decreased as well. Significant enhancement of conductivities in the dopant range $0 \le x \le 0.10$ is also observed. The room temperature conductivity of the sample with $x = 0.06$ is more than four orders of magnitude higher than that of the sample with $x = 0$.

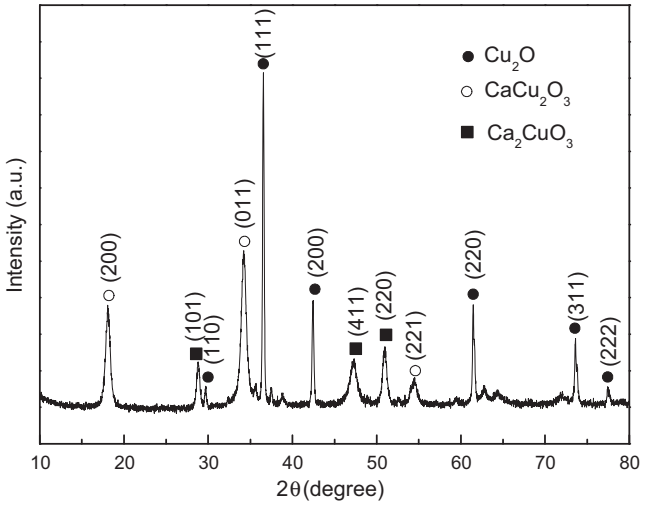

Fig. 6. XRD pattern of sample S5.

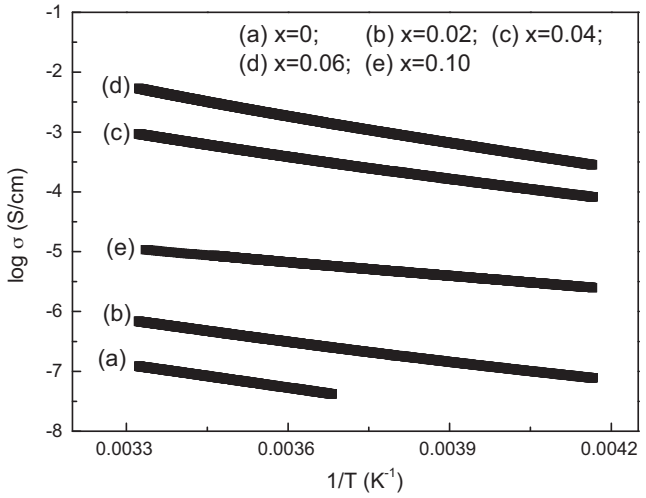

Fig. 7. Temperature dependence of conductivities for $CuY_{1-x}Ca_xO_2$ $(0 \le x \le 0.10)$ samples: (a) $x = 0$; (b) $x = 0.02$; (c) $x = 0.04$; (d) $x = 0.06$; (e) $x = 0.10$.

Acknowledgements

Financial support from the Natural Science Foundation of Anhui province (Project No. 090414169), International Cooperation Program of Anhui province (Project No. 10080703021) and Director's Fund of Hefei Institutes of Physical Science, Chinese Academy of Sciences is gratefully acknowledged.

References

[1] S. Kato, R. Fujimaki, M. Ogasawara, T. Wakabayashi, Y. Nakahara, S. Nakata, Appl. Catal. B-Environ. 89 (2009) 183–188.
[2] W. Ketir, A. Bouguelia, M. Trari, Desalination 244 (2009) 144–152.

[3] H. Dong, Z. Li, X. Xu, Z. Ding, L. Wu, X. Wang, X. Fu, Appl. Catal. B-Environ. 89 (2009) 551–556.
[4] S. Zhou, X.D. Fang, Z.H. Deng, D. Li, W.W. Dong, R.H. Tao, G. Meng, T. Wang, Sensor. Actuators B-Chem. 143 (2009) 119–123.
[5] Z.H. Deng, X.D. Fang, D. Li, S. Zhou, R.H. Tao, W.W. Dong, T. Wang, G. Meng, X.B. Zhu, J. Alloys Compd. 484 (2009) 619–621.
[6] D. Li, X.D. Fang, W.W. Dong, Z.H. Deng, R.H. Tao, S. Zhou, J.M. Wang, T. Wang, Y.P. Zhao, X.B. Zhu, J. Phys. D: Appl. Phys. 42 (2009) 055009–55016.
[7] P.W. Sadik, M. Ivill, V. Craciun, D.P. Norton, Thin Solid Films 517 (2009) 3211–3215.
[8] H.F. Jiang, H.C. Lei, X.B. Zhu, G. Li, Z.R. Yang, W.H. Song, J.M. Dai, Y.P. Sun, Y.K. Fu, J. Alloys Compd. 487 (2009) 404–408.
[9] A.S. Reddy, H.H. Park, G.M. Rao, S. Uthanna, P.S. Reddy, J. Alloys Compd. 474 (2009) 401–405.
[10] D. Li, X.D. Fang, A.W. Zhao, Z.H. Deng, W.W. Dong, R.H. Tao, Vacuum 84 (2010) 851–856.
[11] G. Thomas, Nature 389 (1997) 907–908.
[12] C.E. Benouis, M. Benhaliliba, A. Sanchez Juarez, M.S. Aida, F. Chami, F. Yakuphanoglu, J. Alloys Compd. 490 (2010) 62–67.
[13] D. Li, X.D. Fang, Z.H. Deng, W.W. Dong, R.H. Tao, S. Zhou, J.M. Wang, T. Wang, Y.P. Zhao, X.B. Zhu, J. Alloys Compd. 486 (2009) 462–467.
[14] Z.H. Deng, X.D. Fang, R.H. Tao, W.W. Dong, D. Li, X.B. Zhu, Chin. J. Semiconduct. 29 (2008) 1052–1056.
[15] H.F. Jiang, X.B. Zhu, H.C. Lei, G. Li, Z.R. Yang, W.H. Song, J.M. Dai, Y.P. Sun, Y.K. Fu, J. Alloys Compd. 509 (2011) 1768–1773.
[16] E. Mugnier, A. Barnabé, P. Tailhades, Solid State Ionics 177 (2006) 607–612.
[17] R. Kykyneshi, B.C. Nielsen, J. Tate, J. Li, A.W. Sleight, J. Appl. Phys. 96 (2004) 6188–6194.
[18] M. Beekman, J. Salvador, X. Shi, G.S. Nolas, J. Yang, J. Alloys Compd. 489 (2010) 336–338.
[19] R.L. Hoffman, J.F. Wager, M.K. Jayaraj, J. Tate, J. Appl. Phys. 90 (2001) 5763–5767.
[20] K. Isawa, M. Nagano, K. Yamada, J. Cryst. Growth 237–239 (2002) 783–786.
[21] N. Tsuboi, H. Ohara, T. Hoshino, S. Kobayashi, K. Kato, F. Kaneko, Jpn. J. Appl. Phys. 44 (2005) 765–768.
[22] G.V. Tendeloo, O. Garlea, C. Darie, C.B. Chaillout, P. Bordet, J. Solid State Chem. 156 (2001) 428–436.
[23] D.J. Singh, Phys. Rev. B 77 (2008) 205126–205135.
[24] N. Tsuboi, T. Hoshino, S. Kobayashi, K. Kato, F. Kaneko, Phys. Status Solidi A 203 (2006) 2723–2728.
[25] B.J. Ingram, B.J. Harder, N.W. Hrabe, T.O. Mason, K.R. Poeppelmeier, Chem. Mater. 16 (2004) 5623–5629.
[26] A.M.M. Gadalla, J. White, Br. Ceram. Trans. 62 (1963) 181–190.
[27] G.H. Hou, X.D. Shen, Z.Z. Xu, J. Chin. Ceram. Soc. 33 (2005) 109–114.
[28] M. Trari, A. Bouguelia, Y. Bessekhouad, Sol. Energy Mater. Sol. Cells 90 (2006) 190–202.